Supplementary Information

Lattice Mismatch Induced Strained Phase for Magnetization, Exchange Bias and Polarization in Multiferroic $BiFeO_3$

Rui-Min Yao[1], Chuan-Bao Cao[1,*], Chun-Rui Zheng[1,2] and Qiang Lei[1]

1 Research Center of Materials Science, Beijing Institute of Technology, Beijing 100081, People's. Republic of China.

2 Institute of Material Science and Engineering, Shijiazhuang University of Economics, Shijiazhuang 050031, People's Republic of China.

Corresponding author. Tel.: +86 1068913972; Fax: +86 1068912001;

1. SEM image of surface morphology of BFO ceramics

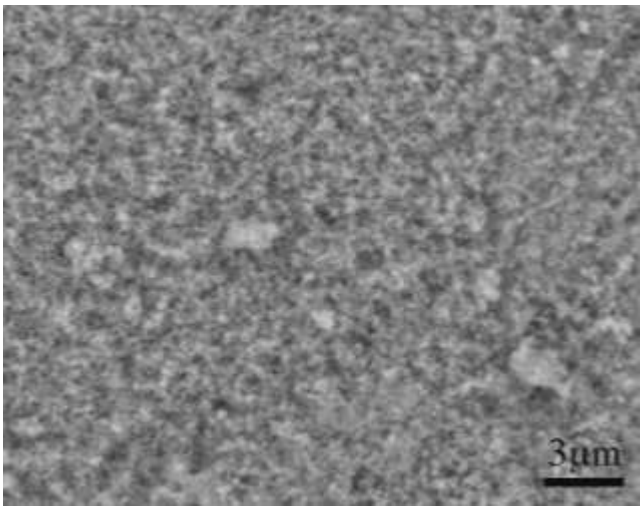

Fig. S1 Surface morphology of BFO ceramics. Many particles with sizes in nanoscale are displayed rather than large microcrystals.

2. The other *P-E* loops of BFO ceramics

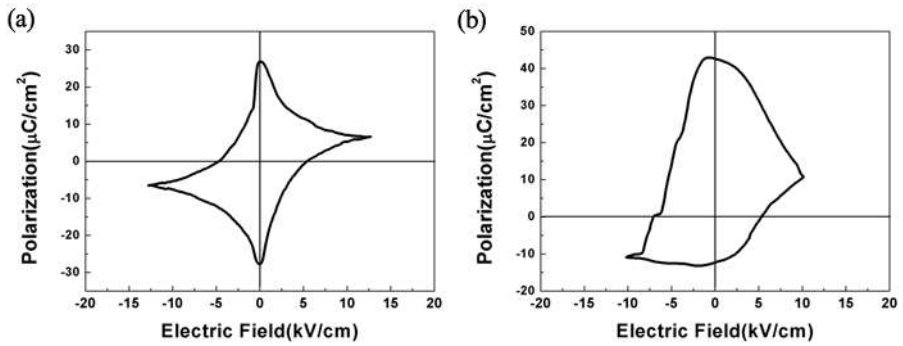

Fig. S2 (a) the first *P-E* loop obtained at the very beginning of the experiment from the first sample we prepared to see if our grain-interface assumption on polycrystal systems is working or not. It indicated the assumption could be achieved. The specific parameters: $2P_r$=54.5 μC cm^{-2}, E_c=5.1 kV/cm. (b) the *P-E* loop obtained from the same sample used in the main text recently under the same test conditions (It has kept in a box for more than two years.). The specific parameters: $2P_r$=56.1 μC cm^{-2}, E_c=6 kV/cm. These results here are close to those in the main text, proved that the *P-E* loop showed in the main text was reproducible.

3. Illustration the formation of distorted layers in BFO ceramics

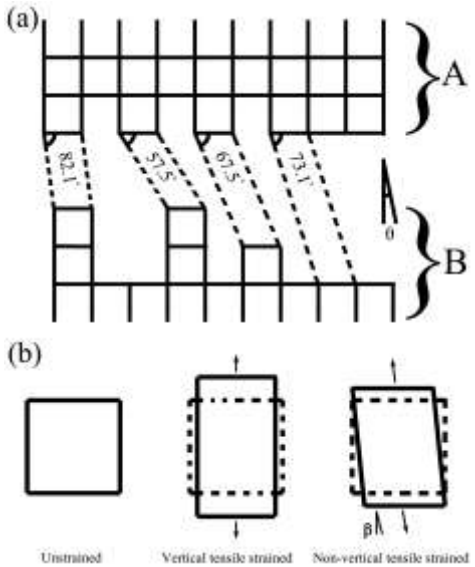

Fig. S3. (a) Diagram for illustration of formation of the tiny zones. Two adjacent particles *A* and *B* are presented using pseudocubic lattices. Particle *A* is default to have a flat surface for easy understanding, while particle *B* is rough and there are some high and low steps on its surface. The misalignment angle β here between the two lattices is settled to be 7.9°. Different angles of the tiny zones would show up with the "help" of roughness of particle *B*. This scenario is agreed with the observed phenomena in Fig. 4c. (b) Diagram of shape changing of a pseudocubic lattice with no strain, vertical tensile strain and the non-vertical tensile strain. The angle θ here is used as a general shifted angle between two adjacent grains.

For easy understanding, we have used a simple pseudocubic lattice to describe a crystal. The growth of the islands is intimate to the status of "substrate" surface. As showed in Fig. S3a, surface of particle *B* is rough and has high and low steps. When "islands" started "homoepitaxial growing" on two BFO "substrates" of *A* and *B*, fresh crystallized lattices would be affected by both of the "substrates". The affection here is a tendency that both "substrates" would like to have fresh crystallized lattices arranged in their own way. Therefore, it leads to the emergency of a tensile strain in the fresh crystallized lattices provided by the two particles. The tensile strain and their shifted angle would lead to lattice distorted due to the existence of misalignment angle β, Fig. S3b.

Moreover, these "islands" of tiny zones will have their individual directions due to both the rough surface of "substrate" *B* and the misalignment angle θ, Fig. S3a. Here, when settled θ as 7.9°, the angles of tiny zones are good agreement with those displayed in Fig. 4c. When a misalignment angle is certain, the roughness of the particle surfaces with high and low steps will make "islands" have different directions.

The misalignment angle changes, the directions of "islands" changes as well. Then, because of the angle β, fresh crystallized lattices will show distorted structures with a lower symmetry than the primary pseudocubic (Fig. S3b). When the lattice is unstrained, it is primary pseudocubic; while under a vertical strain and lattices of two adjacent particles are perfectly matched, it will be stretched along the vertical direction making lattice parameters *c* longer and *a* shorter without change the angle β; if under a non-vertical strain with a misalignment angle θ, the lattice will be distorted not only making lattice parameters c longer and a shorter but change the angle β. This comes out a lower symmetry lattice structure. Therefore, the low growth temperature, low ions mobility, roughness of particle surfaces and the misalignment angle result in the formation of tiny zones with various directions and distorted lattices.

4. Results of XPS and slow scan XRD patterns of selected region

The oxidation state of iron (Fe) in BFO nanoparticles has been investigated by X-ray photoelectron spectroscopy (XPS), the data is fitted, Figure S4a. Peaks at 710.6 eV and 724.9 eV are corresponding to Fe^{3+} and the peak at 718.6 eV was its satellite peak of Fe^{3+} position. There is no detectable signal for the existence of Fe^{2+}, so that the oxidation state of Fe in our BFO ceramics is Fe^{3+} rather than Fe^{2+}. It should be noted that Fe^{2+} is detrimental to the ferroelectric performance of BFO, because it can result in oxygen vacancies that would increase the electrical conductivity.

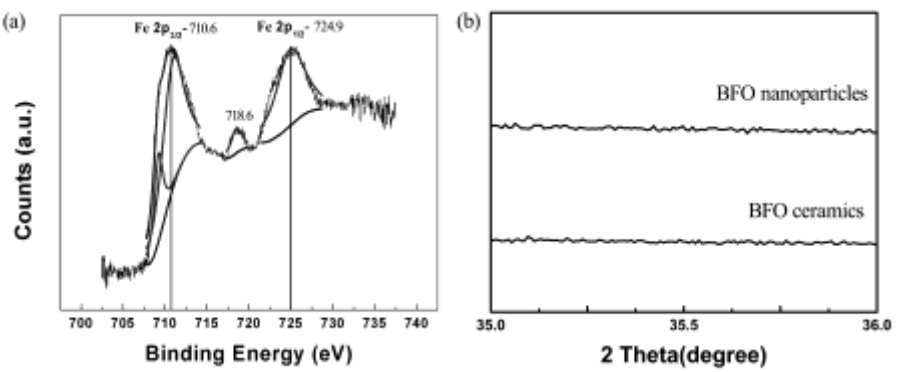

Fig. S4 (a) XPS result of BFO ceramics (b) slow scan XRD patterns of selected region of BFO ceramics and BFO nanoparticles.

Moreover, residual Fe^{2+} can even appear in the form of a second phase in Fe_3O_4 which may "enhance" the magnetization of BFO.[Ref 1] So it is important to remove oxygen vacancies in BFO to prevent the formation of Fe^{2+}. The selected region of XRD test from 35^o to 36^o, where the most intense (311) reflection

from Fe_3O_4 can be expected, showed that there is no detected signal of Fe_3O_4, Figure S4b.

In addition, a low leakage current density of $10^{-7.3}$ A cm^{-2} of BFO ceramics that is comparable with that of BFO films[Ref 2] also indicated the absence of Fe^{2+} ion, because the presence of the Fe^{2+} ion would induce high leakage current.

5. Δ*M*-*H* curves of BFO samples

Δ*M* curves are obtained from isothermal remanence (IRM) and DC demagnetization (DCD) measurements. The IRM measurement records the remanent magnetization (M_r) versus the applied magnetic field (H). But the initial state for the IRM measurement is an alternating current demagnetized state, instead of a fully magnetized state. In a DCD measurement, the film is initially negatively magnetized. The remanent magnetization at zero field is measured as a function of increasing positive applied field. For non-interacting single domain particles, two remanence curves are related to each other by the Wohlfarth relation as follows:

$$M_{DCD}(H)=1-2M_{IRM}(H) \quad (1)$$

Any deviation from this ideal relationship is attributed to intergranular interactions. As a result, $\Delta M(H)$ is defined as:

$$\Delta M=M_{DCD}(H)-[1-2M_{IRM}(H)] \quad (2)$$

Therefore, Δ*M* is a direct measurement of interactions between the grains. Intergranular exchange coupling and magnetic dipolar interaction are two types of intergranular magnetic interaction; the former one would result in positive values of Δ*M* suggesting easy magnetization, while the latter would result in the negative values of Δ*M* indicating difficult magnetization.

The higher the absolute value of Δ*M* is, the stronger the type of interaction would be, vice versa.[Ref 3] Obviously, BFO ceramics had much larger positive value of Δ*M* than BFO nanoparticles. This is suggesting that BFO ceramics had a very strong intergranular exchange coupling during the magnetization.

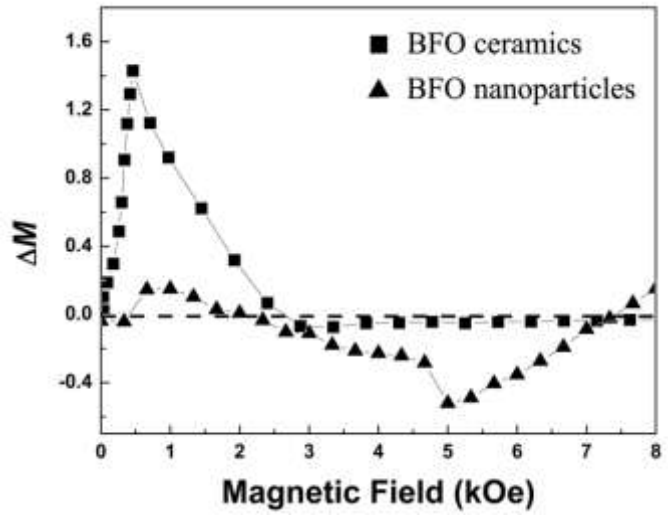

Fig. S5 △*M* behaviors of BFO ceramics and BFO nanoparticles.

6. Leakage current result of BFO ceramics

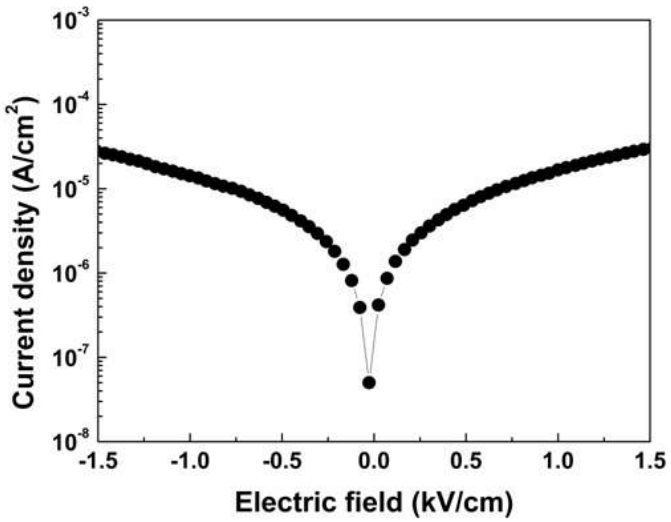

Fig. S6 Leakage current test of BFO ceramics suggests the leakage current is about $10^{-7.3}$ A cm^{-2}.

7. Estimation of the influence of distorted layers on average lattice parameters and magnetization

To estimate the influence of distorted layers on average crystal parameters and magnetization, we have done a series of approximations based on the results of XRD, TEM and HRTEM (Fig. S7).

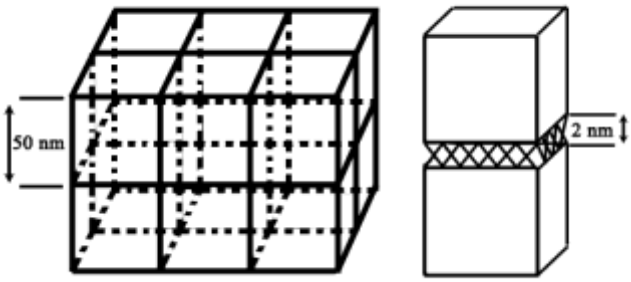

Fig. S7 Approximate BFO nanoparticles to cubes in ceramics that packing in the most compact way and the approximation of distorted layers parameters.

(1). We approximate one ceramic pellet (diameter~5mm, thickness~1mm) as a cuboid (length and width ~5mm, height~1mm). Herein, the cuboid's volume is 2.5×10^{13} nm^3.

(2). We approximate every grain in ceramic as a perfect cubic with side-length of 50nm. Herein, the volume of one grain is 1.25×10^{5} nm^3 and one ceramic has total 2×10^{8} grains.

(3). Grains in ceramic are packing the most compact way.

(4). As one cubic grain has six faces, one ceramic has 1.2×10^{9} faces without consideration of the boundary condition. Each face of one grain can form one distorted layer (thickness~2nm, assume the side-length is 50nm as well) with its adjacent grains. Therefore, 6×10^{8} distorted layers can be formed in one ceramic and their total volume is 3×10^{12} nm^3.

Under these ideal approximations, the volume fraction of distorted layers in one ceramic pellet is 12%.

According to He *et.al.*[Ref. 4], BFO thin films would obtain the magnetic moment 30~50 emu cc^{-1} when the volume fraction of distorted (or highly strained) R-phase is 10~15%. Actually, 10~15% volume fractions was estimated from a small part of the sample (in the top surface of the sample, thickness~5nm) not from the whole thin film attributed to the measuring limitation of X-ray magnetic circular dichroism (XMCD). Therefore, a macroscopic magnetic moment of the whole thin film is ~5 emu cc^{-1} obtained from SQIUD. It suggests that the volume fraction of distorted R-phase in BFO thin film was much lower than 10% and would properly be 1.5% or so.

In our case, the volume fraction of distorted layers is definitely lower than 12% because of the differences between approximations and the practical situation of the BFO ceramics.

(1). Nanograins in BFO ceramics here are not perfect cubes. Their shapes are nearly ellipsoid.

(2). The surface of nanograins are not flat like that of a perfect cube, which we discussed in the main text. These ellipsoid-like nanograins cannot pack in the most compact way.

(3). As showed in Fig.4c, there would be part of incomplete growth in one distorted layer between two adjacent nanograins attributed to the rough surfaces.

Therefore, the real volume fraction of distorted layers in BFO ceramics is lower than 12%.

To further estimate the difference between two BFO samples in lattice parameters and rhombohedra distortion, we have their XRD data quantified by Rietveld refinement with help of TOPAS software (Fig. S8). Moreover, we have further estimated the volume fraction of distorted layers in BFO ceramics based on the refined lattice parameter and the results of Ref.4.

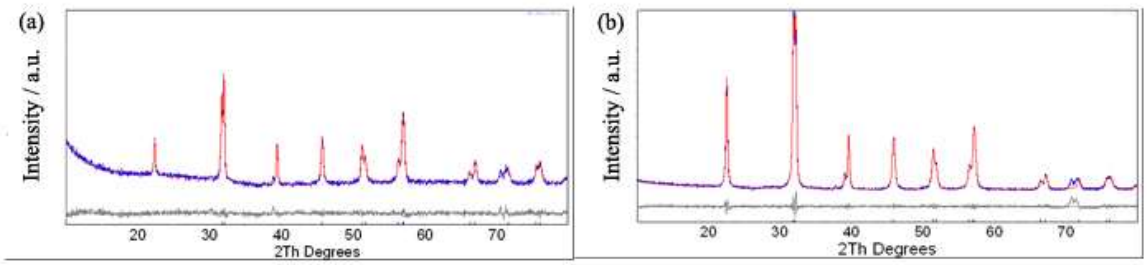

Fig. S8 (a) Rietveld refinement result of XRD pattern of BFO nanoparticles. Lattice parameters are a =5.57898(64) Å, c =6.9336(13) Å. (b) Rietveld refinement result of XRD pattern of BFO ceramics. Lattice parameters are a =5.57669(58) Å, c =6.92665(80) Å.

From refined data of BFO ceramics, lattice parameter of pseudocubic can be calculated as a =3.9439 Å. If taking 100 unit cells as the base and x as the distorted unit cells, we can simply calculate x as follows:

$$[3.78x+(100-x)\times3.95]/100 = 3.9439,\ x\approx3.59.$$

3.78 Å is average lattice value of the distorted layer, 3.95 Å is the measured lattice value of BFO obtained from the result of HRTEM, Fig. 3b. One unit cell has four a, but each adjacent four unit cells share one a. This means the volume fraction of distorted layers in BFO ceramics is ~ 3.59% ([(3.59×4)/(4 ×100)]×100%).

When followed the estimated way according to He *et.al.*[Ref. 4], the magnetic moment of BFO ceramics with a volume fraction of 3.59% is ~ 1.43 emu/g. Although this value is smaller than the measured value of

1.83 emu/g with an error of 21.8%, these two are close. In theory, if the side-length of cuboid BFO nanoparticle down to 40nm, the volume fraction of distorted layers would increase to 15% leading to 5.97 emu/g magnetic moment; furthermore, if the side-length down to 20nm, the volume fraction would be 19.95% results in 7.95 emu/g magnetic moment. Therefore, high magnetic moment can be expected if the volume fraction of distorted layers increased.

8. Characterization of BFO ceramics after sintering at 860°C for 60min

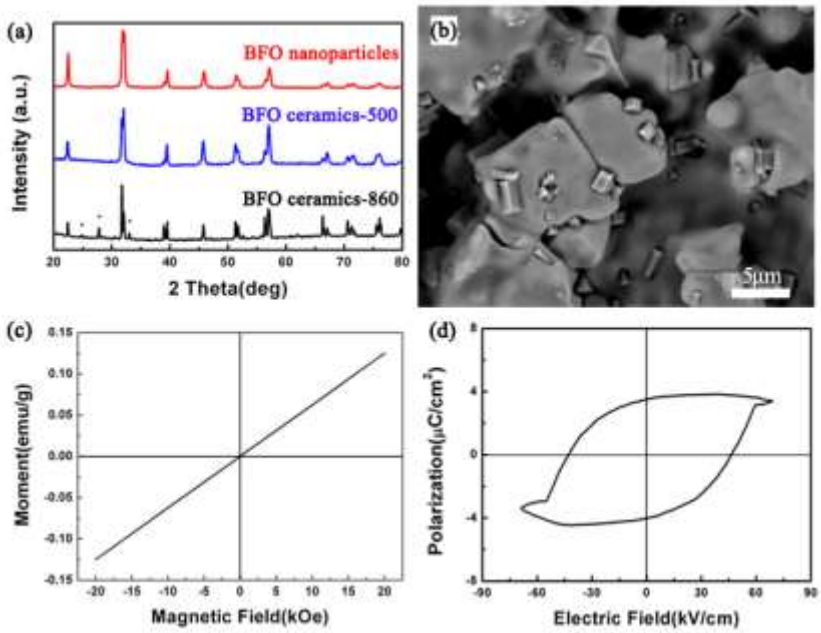

Fig. S9 Characterization of BFO ceramics-860. (a) XRD pattern compared with BFO nanoparticles and BFO ceramics-500 (b) SEM image of surface morphology, the scale bar is 5μm. (c) *M-H* loop (d) *P-E* loop. Note: we use "BFO ceramics-500" to take place "BFO ceramics" used in main text for distinguishing BFO ceramics-860 in this section.

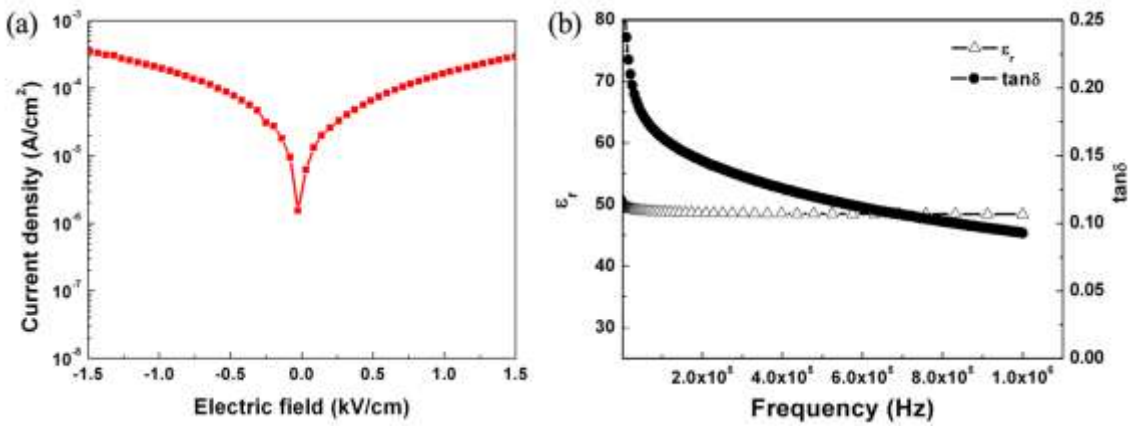

Fig. S10 (a) Leakage current curve of BFO ceramics sintered at 860°C for 60min (b) its corresponding relative dielectric constrant (ε_r) and loss tangent (tanδ) results.

For comparison, BFO ceramics-860 was prepared as follows: Amorphous BFO nanopowders, obtained from organogel after being preheated to 400^{o}C for two times, were grounded in a mortar with one or two water droplets for 20min by hand. Then they were pressed into pellets with a diameter of 5mm and thickness of 1mm. Then put these pellets into a furnace and annealed at 860^{o}C for 60min (ramp-rate 5^{o}C/min).

BFO ceramics-860 have an obvious impurity phase of $Bi_{25}FeO_{40}$ marked by asterisks in Fig.S9a. There is obvious grain growth in BFO ceramics-860 with large crystal sizes above 5μm (Fig.S9b). Besides, some rod-like impurities can be seen clearly. They have an approximately linear behavior indicating the antiferromagnetic behaviour because microparticles made spiral-modulated spin structure unbroken (Fig.S9c). They have a well saturated loop with higher coercive field $E_c \approx 44.6$ kV/cm, $2P_r$ value is very low and only for 7.5 μC cm^{-2} (Fig.S9d) close to the reported value of 6.1 μC cm^{-2} from bulk BFO. They have a higher leakage current ($10^{-5.8}$ A cm^{-2}, Fig.S10a) mainly because of the existence of the impurity. In Fig. S10b, small dielectric constant (ε_r =48.4,) and a high loss tangent (tanδ=0.093) are presented which are both inferior to BFO ceramics obviously.

9. References

1. Vijayanand S, Potdar HS, Joy PA. Appl Phys Lett 2009; 94: 182507.

2. Jang HW, Ortiz D, Baek SH, Folkman CM, Das RR, Shafer P, Chen Y, Pan X, Ramesh R, Eom CB. Adv Mate*r* 2009; 21: 817.

3. Mayo PI, O'Grady K, Kelly PE, Cambridge J, Sanders IL, Yogi T, Chantrell RW. J Appl Phys 1991; 69: 4733.

4. He Q, Chu YH, Heron JT, Yang SY, Liang WI, Kuo CY, Lin HJ, Yu P, Liang CW, Zeches RJ, Kuo WC, Juang JY, Chen CT, Arenholz E, Scholl A, Ramesh R. Nat Comm 2011; 2: 225.